

Green Chemistry

Accepted Manuscript



This is an *Accepted Manuscript*, which has been through the Royal Society of Chemistry peer review process and has been accepted for publication.

Accepted Manuscripts are published online shortly after acceptance, before technical editing, formatting and proof reading. Using this free service, authors can make their results available to the community, in citable form, before we publish the edited article. We will replace this *Accepted Manuscript* with the edited and formatted *Advance Article* as soon as it is available.

You can find more information about *Accepted Manuscripts* in the [Information for Authors](#).

Please note that technical editing may introduce minor changes to the text and/or graphics, which may alter content. The journal's standard [Terms & Conditions](#) and the [Ethical guidelines](#) still apply. In no event shall the Royal Society of Chemistry be held responsible for any errors or omissions in this *Accepted Manuscript* or any consequences arising from the use of any information it contains.

ARTICLE

Electrocatalytic Oxidation of 5-Hydroxymethylfurfural to 2,5-Furandicarboxylic Acid on Supported Au and Pd Bimetallic Nanoparticles[†]

Cite this: DOI: 10.1039/x0xx00000x

Received 00th January 2012,
Accepted 00th January 2012

DOI: 10.1039/x0xx00000x

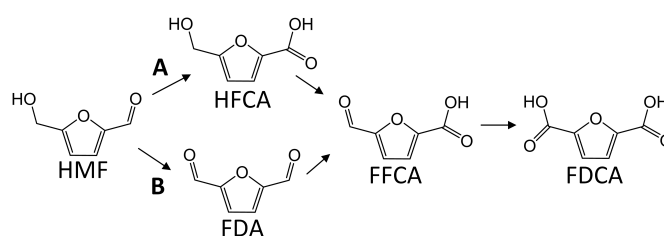
www.rsc.org/

David J. Chadderdon^a, Le Xin^a, Ji Qi^a, Yang Qiu^a, Phani Krishna^a, Karren L. More^b, and Wenzhen Li^{*a}

This work explores the potential-dependent electrocatalytic oxidation of 5-hydroxymethylfurfural (HMF) in alkaline media over supported Au and Pd nanoparticles and demonstrates the synergistic effects of bimetallic Pd-Au catalysts for the selective formation of 2,5-furandicarboxylic acid (FDCA). Results from electrolysis product analysis at various electrode potentials, along with cyclic voltammetry of HMF and its oxidation intermediates, revealed the unique catalytic properties of Pd and Au for competitive oxidation of alcohol and aldehyde side-groups present in HMF. Aldehyde oxidation was greatly favored over alcohol oxidation on Au/C catalyst, which was very active for HMF oxidation to 5-hydroxymethyl-2-furancarboxylic acid (HFCA), however high electrode potentials were required for further oxidation of the alcohol group to FDCA. HMF oxidation on Pd/C followed two competitive routes to FDCA and the pathway was dependent on electrode potential. Oxidation of aldehyde groups occurred much slower on Pd/C than Au/C at low potentials, but was greatly enhanced at increased potentials or by alloying with Au. It was found that Pd-Au bimetallic catalysts achieved deeper oxidized products (FFCA, FDCA) at lower potentials than monometallic catalysts and the product distribution was dependent on electrode potential and surface alloy composition. Bimetallic catalysts with 2:1 and 1:2 Pd-Au molar ratios (Pd₂Au₂/C and Pd₁Au₂/C) exhibited advantages of both single components with facile alcohol and aldehyde group oxidation, resulting in greatly improved HMF conversion rate and selectivity to fully oxidized FDCA.

Introduction

Rapid growth of world population and declining petroleum reserves create a great need for renewable sources of carbon for production of chemicals in the future. Lignocellulosic biomass is an abundant, inexpensive and sustainable resource from which many platform sugars can be derived. New scientific challenges arise in converting these platform sugars because, unlike petroleum feeds, biomass-derived chemicals are often highly-functionalized and new catalytic processes are needed to control the functionality of the final products.¹ Recent research progress has achieved high yield of the important building-block molecule 5-hydroxymethylfurfural (HMF) from six-carbon sugars.²⁻⁵ HMF, which features a furan ring with both alcohol and aldehyde side-groups, has attracted enormous attention, and US DOE has identified HMF as one of the important intermediates for biorenewable chemicals and fuels.⁶⁻⁷ Of particular importance is the oxidation product 2,5-furandicarboxylic acid (FDCA) which is a suitable starting monomer for bio-derived polymeric materials.⁶⁻⁹ The selective oxidation of HMF to FDCA must be



Scheme 1. Possible oxidation reaction pathways of HMF to FDCA.

studied not only for the industrial significance of FDCA, but also as a model for effective catalytic processing of multi-functional molecules from biomass. There is an urgent need to understand the role of catalyst selectivity and its relationship with reaction steps and pathways to design green catalytic processes of the future.

Significant progress has been made in the selective oxidation of HMF in traditional heterogeneous catalytic systems.¹⁰⁻¹⁷ Verdeguer et al. thoroughly studied the selective aerobic oxidation of HMF to FDCA on Pt/C and Pt-Pb/C catalysts under

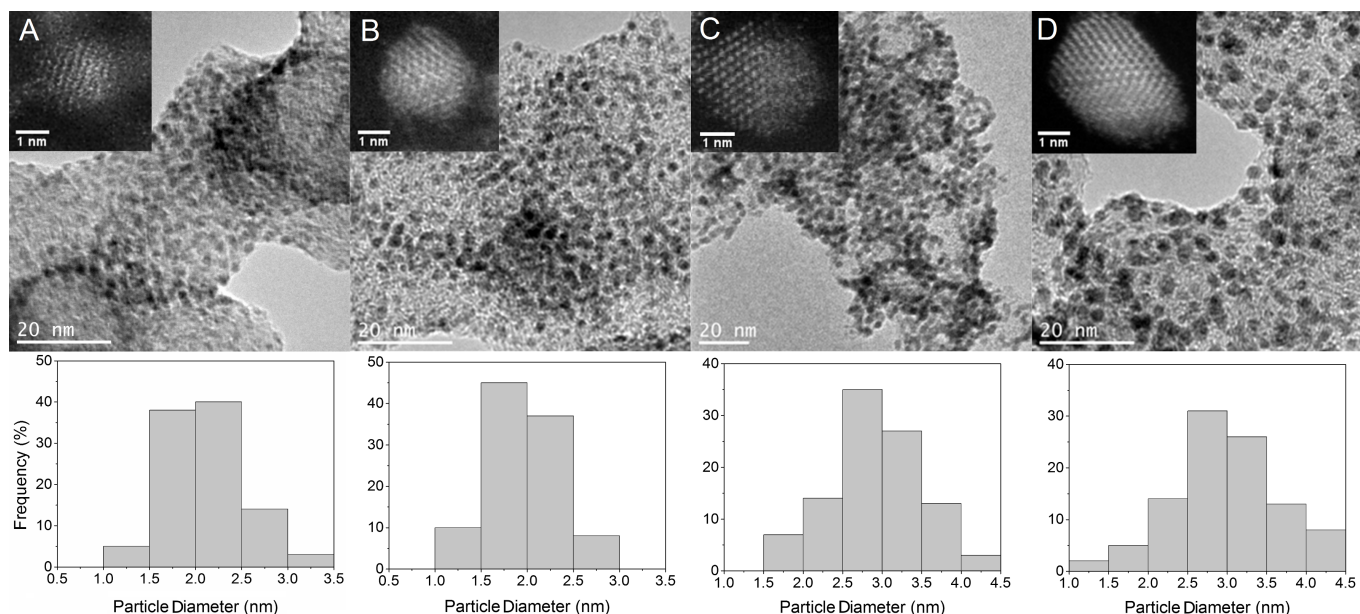


Figure 1. TEM, HAADF-STEM, and particle size histograms of A) Pd/C B) Pd₂Au₁/C C) Pd₁Au₂/C and D) Au/C.

various temperatures and alkaline conditions.¹⁰ They identified two pathways (Scheme 1) to FDCA through either aldehyde oxidation of HMF through 5-hydroxymethyl-2-furancarboxylic acid (HFCA, Path A) or alcohol oxidation of HMF to 2,5-furandicarboxaldehyde (FDA, Path B) and found that the final product distribution was highly dependent on temperature and pH. Casanova and others investigated Au as HMF oxidation catalyst and observed formation of FDCA with high selectivities through the HFCA intermediate.^{11,12,15,17} Later, Davis et al. directly compared supported Au, Pd, and Pt catalysts and found Pd/C and Pt/C were more selective to FDCA (71-79%) than Au/C at complete HMF conversion under identical conditions (6h, 2:1 molar ratio HMF-KOH, 7 bar O₂, 295K).¹⁴ Incomplete oxidation yielding HFCA was observed on Au/C and Davis concluded that higher O₂ pressure and alkaline concentration were required to further oxidize the alcohol group of HFCA to the intermediate 2-formyl-5-furancarboxylic acid (FFCA) and then FDCA. However, discussion of the mechanistic differences of HMF oxidation on Au/C or Pd/C and Pt/C considered only oxidation through the HFCA intermediate (Scheme 1, Path A). Recently, Prati's group found that the activity of supported Au modified with Pt or Pd had extraordinarily increased activity and stability to HMF oxidation and selectivity to FDCA compared to the monometallic catalysts.¹⁶ Furthermore, Au-Pd was more active than Au-Pt and almost reached full conversion to FDCA (2h, 2:1 molar ratio HMF-KOH, 3 bar O₂, 333K). Prati attributed the higher FDCA yield on alloys to an increased resistance to poisoning by adsorbed intermediate species. However, the specific benefits of Pd (or Pt) addition to Au for competitive alcohol and aldehyde group oxidation and the synergistic effect of the alloys remain unclear.

Electrocatalytic oxidation is an alternative reaction system to traditional aerobic oxidation where the driving force is electrochemical potential. The regulation of electrode potential

varies the driving force, and the subsequent surface reactions can be monitored by current measurement. Also, electrochemical systems give rise to the fuel cell, which can simultaneously produce chemical products and renewable electricity.¹⁸⁻²² Electrocatalytic oxidation of HMF on supported noble metal catalysts has recently received attention, however the only published work is limited to a bulk Pt foil electrode, and full oxidation to FDCA was not achieved.²³ The application of supported metal nanoparticle electrocatalysts for HMF oxidation allows parallel research between heterogeneous and electrocatalytic oxidation to help advance both fields. In the past, our group has determined the electrode potential-dependent reaction pathways for selective oxidation of poly-alcohols including ethylene glycol and glycerol on supported nanoparticle catalysts.^{18,19,22,24-26} This research approach is readily expanded to study oxidation of multiple functional groups, as found in HMF.

In the present work, self-prepared monometallic Au/C and Pd/C and bimetallic Pd₂Au₁/C and Pd₁Au₂/C (molar ratios) were applied as electrocatalysts for oxidation of HMF in anion-exchange membrane (AEM) electrolysis flow cell and half-cell reactors to determine the electrode potential-dependent product

Table 1. XRD, TEM, ICP-AES and STEM-EDS results for self-prepared catalysts

Catalyst	Average crystal size ^a [nm]	Average particle size ^b [nm]	Pd: Au molar ratio ^c	Pd: Au molar ratio ^d
Pd/C	2.6	2.1	-	-
Pd ₂ Au ₁ /C	2.2	2.0	1.8 : 1	1.7 : 1
Pd ₁ Au ₂ /C	2.5	2.9	1 : 1.8	1 : 2.3
Au/C	2.8	2.6	-	-

^a from XRD ^b from TEM ^c from ICP-AES ^d from STEM-EDS

distribution and yield. This study elucidates the effects of electrode potential and catalyst metal on the competitive oxidation of aldehyde and alcohol side-groups in alkaline when isolated by the stable furan-ring structure. A reaction pathway is proposed for the aqueous-phase HMF electrocatalytic oxidation on Au/C and Pd/C in alkaline media. The benefit of alloyed Au-Pd catalysts for FDCA production is demonstrated by electrochemical methods and discussed in terms of the proposed reaction pathway and the surface composition and morphology of metallic nanoparticles.

Results and discussion

Physical characterizations of Pd and Au Electrocatalysts

Carbon black supported monometallic Pd/C and Au/C and bimetallic Pd-Au catalysts with 2:1 and 1:2 molar ratios (Pd₂Au₁/C and Pd₁Au₂/C) were prepared by a modified organic phase reduction method.^{20,25,27} The same synthesis conditions, such as surfactant concentration and reduction temperature and duration were used to prepare each catalyst, with only the amount of metal precursors changing with composition. The morphology, structure, and composition of the as-prepared catalysts were analyzed by X-ray diffraction (XRD), transmission electron microscopy (TEM), high-angle annular dark field via aberration-corrected scanning transmission electron microscopy (HAADF-STEM), scanning transmission electron microscopy coupled with high-spatial resolution energy dispersive spectroscopy (STEM-EDS) and inductively coupled plasma atomic emission spectroscopy (ICP-AES). XRD patterns for all catalysts were collected from 15° to 90° and displayed typical face-centered cubic (FCC) patterns with diffraction peaks at ~39°, 46°, 67°, and 80° assigned to the corresponding (111), (200), (220), and (311) facets, respectively (Figure S1, in ESI). From Figure S1, there is a clear shift in peak position with changing metal composition, implying that alloyed crystal structures are present in Pd₂Au₁/C and Pd₁Au₂/C. Average crystal size was calculated from the (220) peak, using the Debye-Scherrer formula and are summarized in Table 1. Typical TEM images, HAADF-STEM images, and corresponding metal particle size histograms are shown in Figure 1. All catalysts have small round-shaped metal particles uniformly distributed on carbon support. The average particle sizes evaluated from TEM were 2.1, 2.0, 2.9 and 2.6 nm for Pd/C, Pd₂Au₁/C, Pd₁Au₂/C, and Au/C, respectively, which is in good agreement with XRD results. The organic phase reduction method achieved very small Pd nanoparticles under these synthesis conditions, while the Au-containing particles were slightly larger and more developed as seen in the HAADF-STEM images. Bulk metal compositions of bimetallic catalysts (Pd₂Au₁/C and Pd₁Au₂/C) were determined by ICP-AES and STEM-EDS and shown in Table 1. Bulk compositions were near the set ratios, indicating that Pd and Au precursors were fully reduced during nanoparticle synthesis. Further characteristics such as the nature of the alloyed phases and surface composition of Pd₂Au₁/C and Pd₁Au₂/C are explored later through electrochemical methods.

Effects of electrode potential and catalyst metal composition on HMF oxidation product distribution in AEM-electrolysis flow cell

The prepared catalysts were investigated for the electrocatalytic oxidation of HMF in an AEM-electrolysis flow cell reactor at applied anode potentials of 0.6, 0.9, and 1.2V vs. RHE and catalyst metal loading of 1 mg cm⁻². Solution of 0.02M HMF (5:1 KOH-HMF molar ratio) passed through the anode reaction volume and product samples were collected for HPLC analysis. HMF conversion and product selectivity of these runs after 1h are shown in Table 2. For all catalysts and tested potentials, FDCA was observed, however HMF conversion and product selectivity were highly dependent on applied anode potential and metal composition. Figure 2 demonstrates the widely varying FDCA molar yield (FDCA selectivity x HMF conversion) after 1h at 0.9V on different catalysts. The bimetallic catalysts demonstrated higher HMF conversion and much greater selectivity to FDCA than monometallic catalysts, with the Au-rich alloy Pd₁Au₂/C being superior over Pd₂Au₁/C. Remarkably, oxidation on Pd₁Au₂/C at 0.9V achieved 83% molar yield of FDCA after 1h, almost three times higher than Pd/C while pure Au/C was nearly inactive to FDCA formation at this potential. Figure 3 shows the strong effect of electrode potential on conversion and product distribution, with the highest conversion to FDCA at 0.9V. It should be noted that HMF conversion rate and FDCA selectivity dropped drastically on Pd-rich catalysts at 1.2V vs. RHE, at which the potential is sufficient for the formation of metal-oxide species which are not active for this reaction. On the other hand, Au/C resists oxidation under the same electrochemical conditions. HMF was fully converted (>99%) after 1h on Au/C at the three tested potentials, however HFCA was the major observed product (S_{HFCA} = 81-98%). Selectivity to FFCA and FDCA significantly increased at 1.2V, indicating that further oxidation of the alcohol-group of HFCA requires high potential on Au/C. In contrast, HMF oxidation on

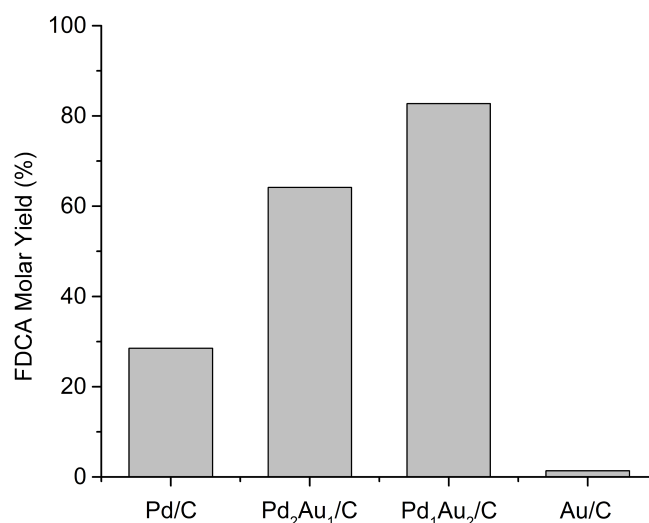


Figure 2. Molar yield of FDCA from oxidation of 0.1M KOH + 0.02M HMF. Reaction conditions: 1 hour; AEM-electrolysis flow cell; anode potential 0.9V vs. RHE; 25°C.

Table 2. HMF oxidation product analysis in AEM-electrolysis flow cell ^a

Catalyst	Potential [V vs. RHE]	C _{HMF} [%]	S _{HFCA} [%]	S _{FDCA} [%]	S _{FFCA} [%]	S _{FDCA} [%]
Pd/C	0.6	75	25	<1	64	11
Pd ₂ Au ₁ /C	0.6	87	30	<1	62	8
Pd ₁ Au ₂ /C	0.6	100	59	-	16	25
Au/C	0.6	100	98	-	<1	1
Pd/C	0.9	97	70	-	<1	29
Pd ₂ Au ₁ /C	0.9	100	35	-	<1	64
Pd ₁ Au ₂ /C	0.9	100	16	-	<1	83
Au/C	0.9	100	98	-	<1	1
Pd/C	1.2	32	71	-	26	3
Pd ₂ Au ₁ /C	1.2	82	61	-	17	22
Pd ₁ Au ₂ /C	1.2	100	60	-	4	36
Au/C	1.2	99	81	-	5	14

^a Reaction conditions: 1 hour; 25 mL of 0.02M HMF, 0.1M KOH solution; flow 20 mL min⁻¹; 25°C; anode catalyst metal loading 1 mg cm⁻². C is conversion. S is molar selectivity.

Pd/C was slower and did not reach complete HMF conversion after 1h, but resulted in higher FDCA production than Au/C at lower potentials. Interestingly, at 0.6V on Pd/C, the major observed product was FFCA (S_{FFCA} = 64%), while at 0.9V the main product was HFCA (S_{HFCA} = 70%). These differences in product distribution between Pd/C and Au/C indicate that the reaction pathway of HMF electrocatalytic oxidation is dependent on catalyst metal and electrode potential. Additional studies of electrocatalytic oxidation of reaction intermediates may clarify these differences and give insight into the benefits of Pd-Au alloyed catalysts for highly active and selective oxidation of HMF to FDCA.

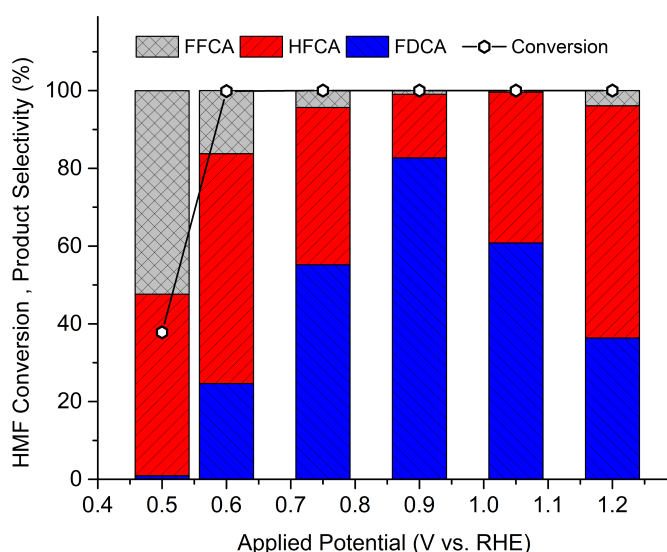


Figure 3. Product distribution on Pd₂Au₁/C for the oxidation of 0.02M HMF in 0.1M KOH. Reaction conditions: 1 hour; AEM-electrolysis flow cell; 25°C.

Onset potential and net peak current density of HMF, HFCA, and FFCA oxidation in half-cell reactor

To further investigate the mechanisms of electro-oxidation of HMF on Pd-Au catalysts, cyclic voltammetry (CV) was conducted with aqueous solutions of 0.1M KOH with and without addition of 0.02M HMF, HFCA, or FFCA. The activities of the prepared catalysts for oxidation of HMF and intermediates were compared in a half-cell reactor by observing oxidation onset potential and peak net current density. Net current density (mA cm⁻²) is defined as the difference of forward-scan anodic current density and blank current density (0.1M KOH only test) and is shown in Figure 4 to visibly demonstrate onset potential and peak current density. Onset potential and peak net current density are summarized in Table 3. Additionally, CVs for HMF, HFCA, and FFCA on Au/C and Pd/C (Figures S2 and S3, respectively in ESI) are included to clearly compare the activities of different functional groups on Pd and Au monometallic catalysts.

Onset of HMF oxidation (Figure 4A), which contains both alcohol and aldehyde groups, occurred at a much lower potential (~260 mV lower) on Au/C than Pd/C, with the alloys falling between the pure catalysts. Similarly, in the low potential range, net current density on pure Au/C was significantly higher than Pd-containing catalysts with HMF electrolyte. The same trend of activity with catalyst composition was observed in the CV of FFCA (Figure 4C), which contains only aldehyde and carboxylic acid groups. These results are consistent with analogous CVs of glyoxylic acid, which features vicinal aldehyde and acid groups on a two-carbon chain, where oxidation onset potential on Au/C was about 140 mV less than on Pd/C (Figure S4, in ESI). To summarize, aldehyde-group oxidation was much easier on Au/C than Pd/C, and the addition of Au to the Pd metal structure greatly facilitated aldehyde oxidation at much lower potentials than pure Pd/C. Alternatively, onset potential of HFCA (Figure 4B), which only contains hydroxyl and carboxylic acid groups, was about 100 mV lower on Pd/C than Au/C and even lower on the Pd-Au alloys. Peak net current density for HFCA oxidation on the alloy catalysts was far superior to mono-metals, reaching about two times higher than Pd/C and eight times higher than Au/C. Interestingly, the CVs for FFCA shows a sharp current increase around 0.8V vs. RHE on Pd/C and Pd₂Au₁/C and a lesser increase on Pd₁Au₂/C. This may indicate a change in reaction mechanism that leads to greatly facilitated aldehyde oxidation at higher potentials on Pd-based catalysts. Furthermore, enhanced aldehyde oxidation on Pd/C at higher potentials may have an effect on reaction pathway, by altering the competitive oxidation of aldehyde and alcohol groups. For comparison, current density of FFCA oxidation on Au/C reached its highest value earlier at 0.71V vs. RHE and gradually decreased at higher potentials.

Evidence from CV of HMF oxidation intermediates provides new insight into the synergistic effect of Au-Pd bimetallic catalysts for selective oxidation, which has been previously studied in both aerobic chemical and electrochemical oxidation systems.²⁸⁻³⁴ The benefit of Au-Pd for selective oxidation of

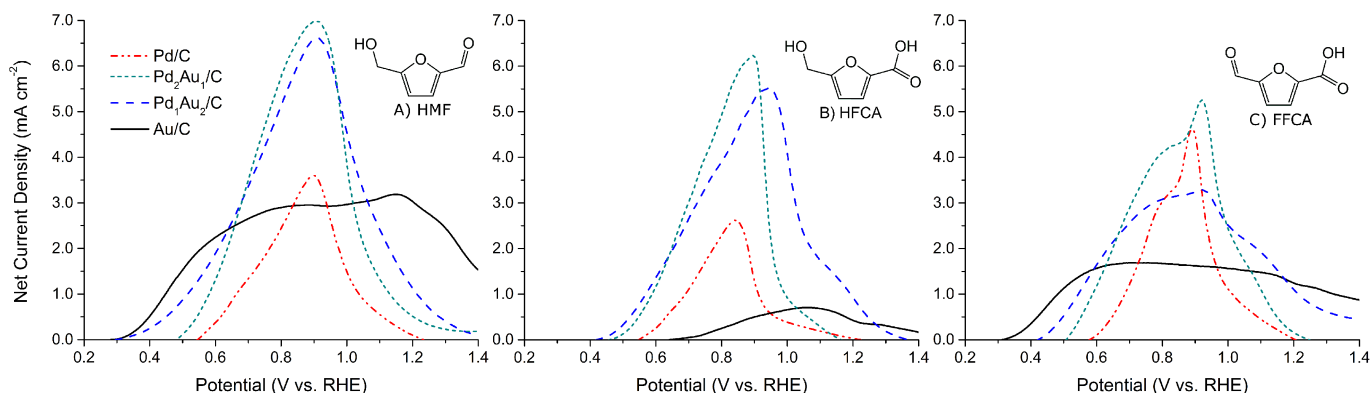


Figure 4. Anodic-scan from half-cell cyclic voltammetry of 0.1M KOH with 0.02M of A) HMF B) HFCA C) FFCA. Net current density is difference of anodic-scan current density and blank current density (0.1M KOH only test). Reaction conditions: 50 mL solution; 25°C; scan rate 50 mV sec⁻¹.

HMF to FDCA is demonstrated by CV to be a combination of facilitated aldehyde oxidation at low potentials and higher activity to alcohol-oxidation.

Reaction pathways of potential-dependent HMF oxidation on supported Pd and Au electrocatalysts

A closer look at time-dependent product distributions reveals further insight into the effects of catalyst metal on reaction mechanism and pathway. Time-dependent HMF conversion and product selectivity for 2h reaction at 0.6V vs. RHE on Au/C and Pd/C are reported in Figure 5 (results on alloyed catalysts are in Figure S5, ESI). On Au/C, HMF was nearly completely converted to HFCA ($S_{HFCA} = 98\%$) after only 30min, followed

by very slow formation of FDCA ($S_{FDCA} = 6\%$ at 2h). In contrast, HMF conversion on Pd/C was significantly slower but resulted in more deeply oxidized products, even at very short reaction times. FFCA was the main observed product ($S_{FFCA} = 52\%$ at 2h) under these conditions with also significant HFCA and FDCA. The intermediate FDA was initially present ($S_{FDA} = 2.5\%$ at 10min) but not detected at 2h reaction. The high selectivity to FFCA and presence of both FDA and HFCA intermediates is evidence that HMF oxidation proceeds by parallel pathways on Pd/C and Au/C under these conditions. Similar evidence for two competitive pathways has been previously reported in traditional heterogeneous catalytic HMF oxidation on Pt/C and Ru(OH)_x on Mg-based supports.^{35,36}

Scheme 2 is the proposed potential-dependent reaction pathway of HMF oxidation in alkaline on Pd/C and Au/C, based on electrochemical results. Electrocatalytic oxidation of HMF on Au/C proceeded by a single pathway, through aldehyde oxidation to HFCA, followed by a potential-sensitive oxidation of the alcohol-group to FFCA, which was rapidly converted to FDCA. Aldehyde oxidation was highly favored over alcohol oxidation on Au/C, as evidenced by the 270 mV negative-shift in onset potential of FFCA in half-cell and the existence of HFCA as the main observed intermediate in AEM-electrolysis flow cell reactor (Table 2 and Figure 5B).

In sharp contrast to Au/C, electrocatalytic oxidation of HMF on Pd/C followed potential-dependent parallel reaction pathways, attributed to its similar onset potentials for alcohol (Table 3: HFCA, 0.55V) and aldehyde oxidation (Table 3: FFCA, 0.58V) and the highly enhanced rate of aldehyde oxidation at higher potentials (Figure 4C). At low potentials, both initial pathways by oxidation of the aldehyde or hydroxyl group of HMF occurred on Pd/C, evidenced by the detection of HFCA and FDA. However, FDA was only detected in early reaction samples (Table 2 and Figure 5A), so it is hypothesized that its formation was followed by fast aldehyde oxidation to FFCA without desorption into the bulk liquid. At 0.6V, the major observed product was FFCA and further oxidation of the aldehyde group to FDCA was relatively slow under these conditions (Figure 5A: $S_{FDCA} = 20\%$, 2h). It should be noted that the non-electrochemical conversion of aldehyde-containing

Table 3. Onset potential and peak current density from CV in half-cell ^a

Species	Catalyst	Onset potential [V vs. RHE]	Peak potential [V vs. RHE]	Peak net ^b current density [mA cm ⁻²]
HMF	Pd/C	0.55	0.90	3.6
	Pd ₂ Au ₁ /C	0.48	0.87	6.9
	Pd ₁ Au ₂ /C	0.30	0.91	6.6
	Au/C	0.29	1.16	3.2
HFCA	Pd/C	0.55	0.84	2.6
	Pd ₂ Au ₁ /C	0.46	0.90	6.2
	Pd ₁ Au ₂ /C	0.42	0.94	5.5
	Au/C	0.64	1.06	0.7
FFCA	Pd/C	0.58	0.89	4.6
	Pd ₂ Au ₁ /C	0.51	0.92	5.2
	Pd ₁ Au ₂ /C	0.42	0.92	3.3
	Au/C	0.31	0.71	1.7

^a Reaction conditions: 50 mL of 0.1M KOH with 0.02M HMF, HFCA, or FFCA; 25°C; 20 μg catalyst loading on glassy carbon electrode; scan rate 50 mV sec⁻¹.

^b Net current density is difference of forward-scan peak current density and blank current density (0.1M KOH only test)

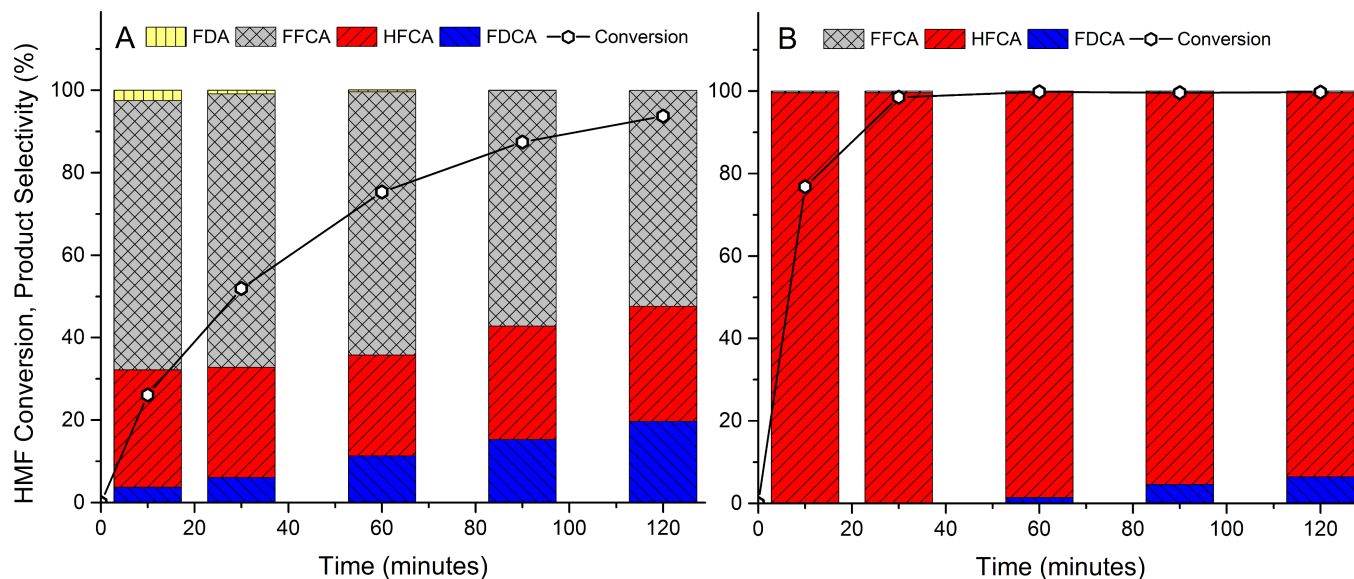
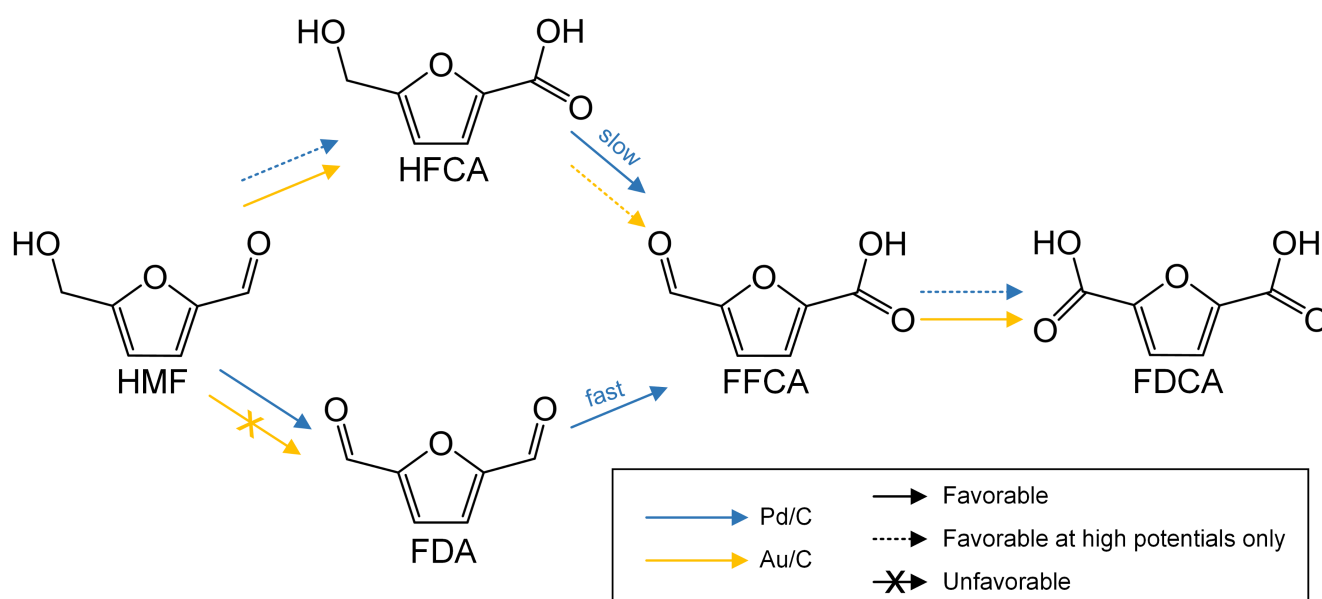


Figure 5. Reaction product profiles for oxidation of HMF over A) Pd/C and B) Au/C including HMF conversion and product selectivity. Reaction conditions: 25 mL of 0.02M HMF, 0.1M KOH solution; flow 20 mL min⁻¹; 25°C; anode potential 0.6V vs. RHE.

species by Cannizzaro's reaction is possible in alkaline solution, but was determined to not be a significant factor under these electrochemical conditions (see ESI, Section 5).^{14,23,37} At higher potentials, aldehyde oxidation was greatly enhanced on Pd/C, as evidenced in cyclic voltammetry of FFCA (Figure 4C), making the initial oxidation of HMF to HFCA highly favorable over the alcohol-oxidation pathway. The alcohol group on HFCA was relatively non-reactive and consequently HFCA was the major observed product on Pd/C at 0.9V (Table 2: $S_{HFCA} = 70\%$, 1h). Meanwhile, the route of HMF oxidation through FDA becomes a more minor pathway and as a result of accelerated aldehyde oxidization at higher potentials, any FDA or FFCA formed would rapidly oxidize to FDCA, which explains the lack of

aldehyde-containing intermediates detected on Pd/C (Table 2: $S_{FFCA} < 1\%$, $S_{FDA} = 0\%$, 1h at 0.9V).

After clarifying the reaction pathway and slow steps on pure Au/C and Pd/C, some conclusions can be made about the benefit of alloyed Au-Pd catalysts for FDCA production. At low potentials, HMF oxidation of Pd/C stopped at FFCA. As shown from cyclic voltammetry, the addition of Au greatly facilitated aldehyde oxidation at lower potentials. This resulted in more favorable aldehyde oxidation of HMF to HFCA and faster oxidation of FFCA to FDCA, which is consistent with final product analysis (Table 1). Both alloy catalysts had increased HMF conversion rate and HFCA selectivity, and the Au-rich Pd₁Au₂/C demonstrated significant further oxidation of FFCA to



Scheme 2. Proposed reaction pathways of HMF oxidation on Pd/C and Au/C electrocatalysts in alkaline media.

FDCA even at 0.6V ($S_{\text{FDCA}} = 25\%$ at 1h). At higher potentials, HMF oxidation on both Pd/C and Au/C yielded HFCA as the major product. From cyclic voltammetry, oxidation of the alcohol group in HFCA on alloyed catalysts was shown to have much lower onset potential and higher peak current density than both Au and Pd (Table 3). In the AEM-electrolysis flow cell this resulted in increased activity to HFCA oxidation and greatly increased selectivity to FDCA. The synergy of Au-Pd alloyed catalysts for facile aldehyde oxidation at low potentials and enhanced alcohol oxidation activity was demonstrated in half-cell and AEM-electrolysis flow cell reactors and provides a promising catalyst for selective FDCA production from HMF.

Effects of structure and morphology on Pd-Au bimetallic electrocatalysts activity for HMF oxidation

It is well-known that bimetallic Pd-Au catalysts have greatly enhanced activity over their monometallic components for many applications, although the promotional role of Pd or Au is under debate. Bimetallic systems can introduce morphological and structural changes including the dilution of one atom type on the surface, different lattice parameters, possible electron charge transfer between different metal atoms, and formation of phase boundaries.³⁸ Previous works have proposed that isolated Pd atoms make highly active catalytic sites with decreased species adsorption energy compared to pure Pd crystals, and therefore that the role of Au is dilute and stabilize surface Pd.³⁸⁻⁴² Surface metal composition, which may vary greatly from bulk composition, is a critical factor in catalyst activity and selectivity and therefore additional analysis was needed to characterize the surface morphology of supported Pd-Au alloy catalysts for HMF oxidation.

The surface atomic compositions of Pd-Au alloys were determined by electrochemical methods first proposed by Rand and Woods.⁴³ In cyclic voltammetry, a distinct reduction peak is observed in the cathodic scan direction corresponding to the

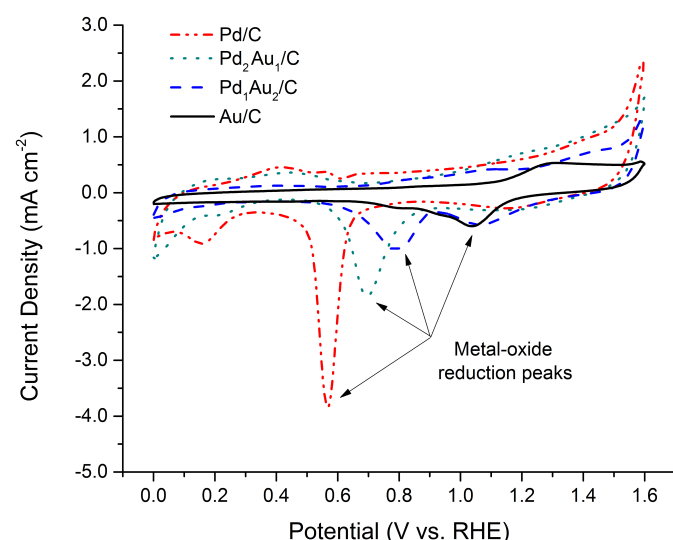


Figure 6. Cyclic voltammetry in 0.1M KOH for electrochemical determination of surface metal composition. Reaction conditions: 50 mL electrolyte; 25°C; 20 μg catalyst loading on glassy carbon electrode; scan rate 50 mV sec^{-1} .

reduction of metal-oxides formed on the catalyst surface during the anodic scan. The peak position depends on the catalyst surface composition, and therefore can be used to determine the nature of surface alloy structures present in Pd-Au.^{43,44} Cyclic voltammetry was performed in 0.1M KOH electrolyte and the resulting curves for alloyed catalysts and pure Pd/C and Au/C are shown in Figure 6. Pd/C shows a sharp Pd-oxide reduction peak at 0.57V and Au/C shows a shallow Au-oxide reduction peak at 1.04V vs. RHE, which are in agreement with our previously reported results.²⁷ The alloyed catalysts had reduction peaks shifted away from the monometallic catalysts at 0.70 and 0.79V vs. RHE which corresponds to 72 and 53 at.% Pd for Pd₂Au₁/C and Pd₁Au₂/C, respectively, according to Rand and Wood's method (Details in ESI Section 6). These alloyed surfaces were found to be significantly more Pd-enriched than the bulk composition (from ICP: 64 and 36 at.%, and STEM-EDS: 63 and 30 at.%), a phenomenon which has previously been observed for Pd-Au particles synthesis by wet-chemistry methods.^{45,46} Furthermore, it is interesting to observe a second reduction peak on Pd₁Au₂/C at the signature potential for pure Au, indicating that two metallic phases were present on the catalyst surface, one alloyed Pd-Au phase and one non-alloyed Au phase. However, only one reduction peak was observed for Pd₂Au₁/C, which suggests that a single alloyed phase was present on the catalyst surface and monometallic phases were absent.

The proposed beneficial role of Au is to isolate and stabilize Pd sites on the surface, and therefore higher surface Au composition (47 at.% surface Au in Pd₁Au₂ alloy vs. 28 at.% surface Au in Pd₂Au₁ alloy) is desired to increase the fraction of isolated Pd sites and catalytic activity. This was evidenced by Prati's group, who found increased turn-over frequencies (TOF) for glycerol oxidation with increasing Au-content up to 90% Au, beyond which TOF decreased sharply.⁴² Enhanced activity to HMF oxidation on Pd₁Au₂/C compared to Pd₂Au₁/C can therefore partially be attributed to its higher surface Au composition in the alloy phase and increased number of isolated Pd sites. Additionally, electrochemical techniques provided evidence of pure Au regions on the Pd₁Au₂/C metal surface, leading to a unique two-phase catalyst which we hypothesize further contributes to its superior activity and selectivity. Au/C was found to be highly active for aldehyde oxidation at all potentials but poor for alcohol oxidation at potentials <1.2V, so we propose that pure Au regions can promote aldehyde adsorption and oxidation, while Pd-rich alloyed regions promote alcohol oxidation. The intimate contact of Au and alloyed Pd-Au regions provides a bi-functional surface for aldehyde and alcohol oxidations which are both necessary to efficiently obtain fully oxidized FDCA.

Experimental

Catalyst synthesis

Carbon black supported Pd, Pd-Au, and Au nanoparticles were synthesized by reduction of metal precursors Pd(acac)₂ (Sigma-Aldrich, 99%) and AuCl₃ (Sigma-Aldrich, 99%) followed by

deposition on carbon black support (Vulcan XC-72, Cabot). Typically, precursors were dissolved in 16 mL 1-octadecene (Sigma Aldrich, 90%) and 4 mL oleylamine (Aldrich Chemistry, 70%) and heated to 80°C under nitrogen flow. The precursors were added to give 2:1 and 1:2 Pd/Au molar ratios for the bimetallic nanoparticles. 1.7 mL LiEt₃BH (1.0M in THF, Acros Organics) was injected to rapidly precipitate metal nanoparticles and after 10min the solution was cooled to room temperature before drop-wise transfer to a well-stirred dispersion of carbon black in hexane and ethanol. The amount of carbon black was controlled to give approximately 40 wt.% metal in the catalyst. The final catalysts were cleaned with ethanol, separated by vacuum filtration and dried overnight.

Catalyst characterizations

Prepared catalysts were characterized by TEM (JEOL 2010) with an operating voltage of 200 kV. XRD patterns were obtained with a Scintag XDS-2000 θ/θ diffractometer using CuK α radiation ($\lambda=1.5406$), with a tube current of 35 mA and a tube voltage of 45 kV. HAADF-STEM and STEM-EDS were performed on a Hitachi HF-3300 TEM-STEM with Bruker silicon drift detector (SDD). Catalysts were digested in aqua regia (HCl:HNO₃ volume ratio 3:1) and analyzed by a PerkinElmer ICP-AES, model 7000 DV to verify bulk metal loading and composition.

Half-cell tests

Cyclic voltammetry was performed in a glass reactor with a three-electrode setup controlled by potentiostat (Versastat MC, Princeton Applied Research). Prepared catalysts were dispersed in isopropanol by ultrasonication to form a uniform ink (1.0 mg mL⁻¹). With a micro-syringe, 20 μ L of ink were deposited onto a polished and cleaned glassy-carbon electrode with working area of 0.1963 cm². Hg/HgO (1.0M KOH) reference electrode and Pt-wire counter electrode were used. Typically, the cell was loaded with 50 mL solution of 1.0 mmol HMF (Sigma-Aldrich, $\geq 99\%$) and 5.0 mmol KOH (Sigma-Aldrich, $\geq 85\%$) in de-ionized water. Cyclic voltammetry was performed at a constant sweep rate of 50 mV sec⁻¹ in alkaline solution with and without addition of HMF at 25°C with nitrogen bubbling. Additional tests were performed with 1.0 mmol HFCA (Matrix Scientific, $\geq 99\%$) and FFCA (TCI America, $\geq 98\%$).

AEM-electrolysis flow cell tests

A custom-made reactor was built with a membrane-electrode assembly (MEA) consisting of a solid anion-exchange membrane (AEM, Tokuyama) mechanically sandwiched between anode and cathode catalyst layers on carbon cloth. Self-prepared Pd/C, Au-Pd/C, and Au/C served as anode catalysts, while commercial Pt/C (40 wt.% Pt, ETEK) was the cathode catalyst. Catalyst and PTFE was dispersed in isopropanol with by ultrasonication to form a uniform ink (10 mg catalyst mL⁻¹) which was painted onto the carbon cloth with a spray gun. The mass of catalyst on carbon cloth was calculated to give a metal (Au, Pd, Pt) loading of 1 mg cm⁻². After drying, the catalyst to PTFE mass ratio was 9:1. Hg/HgO (1.0M KOH) reference

electrode was inserted through a hole in the anode compartment, allowing the anode potential to be regulated and monitored by potentiostat (Versastat MC, Princeton Applied Research). Additional details of electrolysis flow cell design can be found in our previous works.^{26,47,48} Product samples were taken throughout the test for analysis by HPLC (Agilent 1100, Alltech OA-1000 column, 60°C) equipped with RID (Agilent G1362A) and VWD (Agilent G1314A, 220 nm) and a 5.0 mM aqueous H₂SO₄ mobile phase (0.3 mL min⁻¹).

Conclusions

Electrocatalytic oxidation of HMF in an AEM-electrolysis flow cell reactor with product analysis at varying electrode potentials, along with cyclic voltammetry of HMF, HFCA, and FFCA provided direct evidence of Au-Pd synergistic effect for HMF electro-oxidation for FDCA production, and revealed the unique catalytic properties of Pd and Au for competitive oxidation of alcohol and aldehyde groups present in HMF. The observed product distribution from the AEM-electrolysis flow cell was highly dependent on electrode potential and catalyst surface composition. We have reported the electrode potential-dependent pathway for electrocatalytic oxidation of HMF in alkaline media over supported Au and Pd nanoparticles. Under these electrochemical conditions, Au/C favored HMF oxidation to HFCA, while oxidation on Pd/C followed two competitive pathways to FDCA. Aldehyde oxidation was greatly favored over alcohol oxidation on Au/C, but required higher potentials to proceed rapidly on Pd/C. Bimetallic catalysts (Pd₂Au₁/C and Pd₁Au₂/C) achieved much higher FDCA yield, attributed to altered surface composition and morphology. Introducing Au to the Pd surface led to more facile aldehyde oxidation at low potentials and enhanced alcohol oxidation activity compared to both single elements. The combined benefits of Pd-Au alloys for the selective production of FDCA from HMF were demonstrated in electrochemical systems and this approach may be expanded to the rational design other highly active and selective catalysts for multi-functional group oxidation in green processes for the future.

Acknowledgements

We acknowledge partial financial support from the US National Science Foundation (CBET-1159448) and Michigan Tech Research Excellence Fund (E49290). Ji Qi is grateful to the Chinese Scholarship Council for support.

Notes and references

^a Chemical Engineering Department

Michigan Technological University

1400 Townsend Drive, Houghton, MI 49931 (USA)

E-mail: wzli@mtu.edu

^b Material Science and Technology Division

Oak Ridge National Laboratory

Oak Ridge, Tennessee 37831 (USA)

- † Electronic Supplementary Information (ESI) available. See DOI: 10.1039/b000000x/
- 1 W. J. Medlin, *ACS Catal.*, 2011, **1**, 1284-1297.
 - 2 J. N. Chheda, G. W. Huber and J. A. Dumesic, *Angew. Chem. Int. Ed.*, 2007, **46**, 7164-7183.
 - 3 J. N. Chheda, Y. Roman-Leshkov and J. A. Dumesic, *Green Chem.*, 2007, **9**, 342-350.
 - 4 A. Corma, S. Iborra and A. Velty, *Chem. Rev.*, 2007, **107**, 2411-2502.
 - 5 Y. Roman-Leshkov, J. N. Chheda and J. A. Dumesic, *Science*, 2006, **213**, 1933-1937.
 - 6 T. Werpy and G. Peterson, *NREL/TP-510-35523*, 2004.
 - 7 J. J. Bozell and G. R. Petersen, *Green Chem.*, 2010, **12**, 539-554.
 - 8 A. Gandini, A. J. D. Silvestre, C. P. Neto, A. F. Sousa and M. Gomes, *J. Polym. Sci., Part A: Polym. Chem.*, 2009, **47**, 295-298.
 - 9 X. Tong, Y. Ma and Y. Li, *Appl. Catal., A*, 2010, **385**, 1-13.
 - 10 P. Verdeguer, N. Merat and A. Gaset, *J. Mol. Catal.*, 1993, **85**, 327-344.
 - 11 I. O. Casanova, S. Iborra and A. Corma, *ChemSusChem*, 2009, **2**, 1138-1144.
 - 12 Y. Y. Gorbanev, S. K. Klitgaard, J. M. Woodley, C. H. Christensen and A. Riisager, *ChemSusChem*, 2009, **2**, 672-675.
 - 13 A. A. Rosatella, S. P. Simeonov, R. F. M. Fradea and C. A. M. Afonso, *Green Chem.*, 2010, **13**, 754-793.
 - 14 S. E. Davis, L. R. Houk, E. C. Tamargo, A. K. Datye and R. J. Davis, *Catal. Today*, 2011, **160**, 55-60.
 - 15 T. Pasini, M. Piccinini, M. Blosi, R. Bonelli, S. Albonetti, N. Dimitratos, J. A. Lopez-Sanchez, M. Sankar, Q. He, C. J. Kiely, G. J. Hutchings and F. Cavanha, *Green Chem.*, 2011, **13**, 2091-2099.
 - 16 A. Villa, M. Schiavoni, S. Campisi, G. M. Veith and L. Prati, *ChemSusChem*, 2013, **6**, 609-612.
 - 17 E. Taarning, I. S. Nielsen, K. Egeblad, R. Madsen and C. H. Christensen, *ChemSusChem*, 2008, **1**, 75-78.
 - 18 L. Xin, Z. Zhang, Z. Wang and W. Li, *ChemCatChem*, 2012, **4**, 1105-1114, S1105/1101-S1105/1106.
 - 19 Z. Zhang, L. Xin and W. Li, *Appl. Catal., B*, 2012, **119-120**, 40-48.
 - 20 Z. Zhang, L. Xin and W. Li, *Int. J. Hydrogen Energy*, 2012, **37**, 9393-9401.
 - 21 J. Qi, L. Xin, Z. Zhang, K. Sun, H. He, F. Wang, D. Chadderdon, Y. Qiu, C. Liang and W. Li, *Green Chem.*, 2013, **15**, 1133-1137.
 - 22 J. Qi, L. Xin, D. J. Chadderdon, Y. Qiu, Y. Jiang, N. Benipal, C. Liang and W. Li, *Appl. Catal., B*, 2014, **154-155**, 360-368.
 - 23 K. R. Vuyyuru and P. Strasser, *Catal. Today*, 2012, **195**, 144-154.
 - 24 L. Xin, Z. Zhang, J. Qi, D. J. Chadderdon and W. Li, *Appl. Catal., B*, 2012, **125**, 85-94.
 - 25 Z. Zhang, L. Xin, J. Qi, Z. Wang and W. Li, *Green Chem.*, 2012, **14**, 2150-2152.
 - 26 Z. Zhang, L. Xin, J. Qi, D. J. Chadderdon, K. Sun, K. M. Warsko and W. Li, *Appl. Catal., B*, 2014, **147**, 871-878.
 - 27 Z. Zhang, L. Xin, J. Qi, D. J. Chadderdon and W. Li, *Appl. Catal., B*, 2013, **136-137**, 29-39.
 - 28 C. L. Bianchi, P. Canton, N. Dimitratos, F. Porta and L. Prati, *Catal. Today*, 2005, **102-103**, 203-212.
 - 29 N. Dimitratos, F. Porta and L. Prati, *Appl. Catal., A*, 2005, **291**, 210-214.
 - 30 N. Dimitratos, A. Villa, D. Wang, F. Porta, D. Su and L. Prati, *J. Catal.*, 2006, **244**, 113-121.
 - 31 D. I. Enache, J. K. Edwards, P. Landon, B. Solsona-Espriu, A. F. Carley, A. A. Herzing, M. Watanabe, C. J. Kiely, D. W. Knight and G. J. Hutchings, *Science*, 2006, **311**, 362-365.
 - 32 Y. Wook Lee, M. Kim, Y. Kim, S. Wook Kang, J.-H. Lee and H. Woo, *J. Phys. Chem. C*, 2010, **114**, 7689-7693.
 - 33 G. L. Brett, Q. He, C. Hammond, P. J. Miedziak, N. Dimitratos, M. Sankar, A. A. Herzing, M. Conte, J. A. Lopez-Sanchez, C. J. Kiely, D. W. Knight, S. H. Taylor and G. J. Hutchings, *Angew. Chem. Int. Ed.*, 2011, **123**, 10318-10321.
 - 34 L. Kesavan, R. Tiruvalam, M. H. A. Rahim, M. I. bin Saiman, D. I. Enache, R. L. Jenkins, N. Dimitratos, J. A. Lopez-Sanchez, S. H. Taylor, D. W. Knight, C. J. Kiely and G. J. Hutchings, *Science*, 2011, **331**, 195-199.
 - 35 Y. Y. Gorbanev, S. Kegnæs and A. Riisager, *Catal. Lett.*, 2011, **141**, 1752-1760.
 - 36 H. A. Rass, N. Essayem and M. Besson, *Green Chem.*, 2013, **15**, 2240-2251.
 - 37 E.-S. Kang, D. W. Chae, B. Kim and Y. G. Kim, *J. Ind. Eng. Chem.*, 2012, **18**, 174-177.
 - 38 F. Maroun, F. Ozanam, O. M. Magnussen and R. J. Behm, *Science* 2001, **293**, 1811-1814.
 - 39 R. Meyer, C. Lemire, S. K. Shaikhutdinov and H. J. Freund, *Gold Bull.*, 2004, **37**, 72-124.
 - 40 S. J. Mejia-Rosales, C. Fernandez-Navarro, E. Perez-Tijerina, D. A. Blom, L. F. Allard and M. J. Yacamán, *J. Phys. Chem. C*, 2007, **111**, 1256-1260.
 - 41 M. Chen and D. W. Goodman, *Chin. J. Catal.*, 2008, **29**, 1178-1186.
 - 42 D. Wang, A. Villa, F. Porta, L. Prati and D. Su, *J. Phys. Chem. C*, 2008, **112**, 8617-8622.
 - 43 D. Rand and R. Woods, *J. Electroanal. Chem.*, 1972, 57-69.
 - 44 M. Mougnot, A. Caillard, M. Simoes, S. Baranton, C. Coutanceau and P. Brault, *Appl. Catal., B*, 2011, **107**, 372-379.
 - 45 M. Simoes, S. Baranton and C. Coutanceau, *J. Phys. Chem. C*, 2009, **113**, 13369-13376.
 - 46 M. Simoes, S. Baranton and C. Coutanceau, *Appl. Catal., B*, 2010, **93**, 354-362.
 - 47 L. Xin, Z. Zhang, J. Qi, D. J. Chadderdon, Y. Qiu, K. M. Warsko and W. Li, *ChemSusChem*, 2013, **6**, 674-686.
 - 48 Y. Qiu, L. Xin, D. J. Chadderdon, J. Qi, C. Liang and W. Li, *Green Chem.*, 2014.

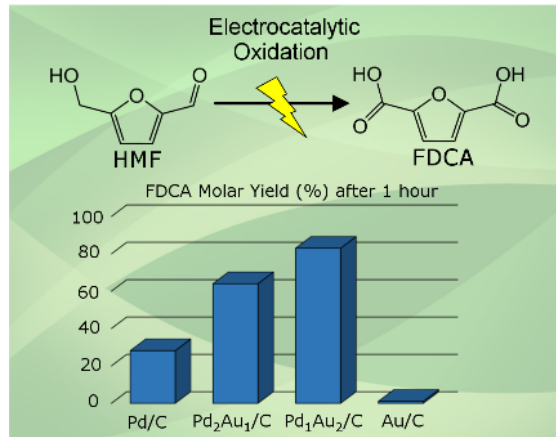
Table of Contents: Electrocatalytic Oxidation of 5-Hydroxymethylfurfural to 2,5-Furandicarboxylic Acid on Supported Au and Pd Bimetallic Nanoparticles

David J. Chadderdon^a, Le Xin^a, Ji Qi^a, Yang Qiu^a, Phani Krishna^a, Karren L. More^b, and Wenzhen Li^{*a}

^a Chemical Engineering Department Michigan Technological University 1400 Townsend Drive, Houghton, MI 49931 (USA) E-mail: wzli@mtu.edu

^b Material Science and Technology Division Oak Ridge National Laboratory Oak Ridge, Tennessee 37831 (USA)

Text and graphical abstract for Table of Contents (TOC)*:



*Higher quality figure included in ZIP file

Electrocatalytic oxidation of HMF to FDCA was achieved on Pd/C, Au/C and Pd-Au/C catalysts and the synergistic effect of Pd-Au alloying is clearly demonstrated with electrochemical methods.

Word count: 27 words